Growth, structure, and magnetic properties of artificially layered NiMn in contact to ferromagnetic Co on $Cu_3Au(001)$

*Tauqir Shinwari Ismet Gelen Melek Villanueva Ivar Kumberg Yasser A. Shokr M. Yaqoob Khan Wolfgang Kuch**

T. Shinwari, I. Gelen, I. Kumberg, W. Kuch
Institut für Experimentalphysik, Freie Universität Berlin, Arnimallee 14, 14195 Berlin, Germany
Email Address: kuch@physik.fu-berlin.de
M. Villanueva
Group of Permanent Magnets and Applications, IMDEA Nanoscience, 28049 Madrid, Spain
Y. A. Shokr
Institut für Experimentalphysik, Freie Universität Berlin, Arnimallee 14, 14195 Berlin, Germany and
Faculty of Science, Department of Physics, Helwan University, 17119 Cairo, Egypt
M. Y. Khan
Department of Physics, Kohat University of Science and Technology, Kohat 26000, Khyber Pakhtunkhwa, Pakistan

Keywords: *Artificial fabrication, Alternate monoatomic layer deposition, Exchange bias, Disordered alloy NiMn films*

Single-crystalline antiferromagnetic artificially layered [Ni/Mn] films of different thicknesses, covered by ferromagnetic Co layers, have been deposited on $Cu_3Au(001)$. Their structural and magnetic properties are characterized by low-energy electron diffraction (LEED) and magneto-optical Kerr effect, respectively, and compared with disordered Ni_xMn_{1-x} alloy films with the same Ni/Mn ratio and the same film thickness. LEED I(V) curves show that the perpendicular interatomic lattice distance is decreased in the artificially layered [Ni/Mn] samples in comparison to the disordered Ni_xMn_{1-x} alloy films. At the same time, the artificially layered [Ni/Mn] films exhibit higher coercivity and exchange bias of the adjacent Co layer compared to those of Ni_xMn_{1-x}/Co. This is discussed as a consequence of the different interatomic lattice distance, presumably caused by an ordered buckling in the artificially layered [Ni/Mn] samples, leading to a stronger interlayer exchange coupling.

1 Introduction

Over the past few decades, tailoring the properties of functional materials at the atomic scale has been the focus of a large part of materials science research. The technological development enabled scientists and engineers to design materials with atomic-level precision [1–3]. The motivation behind the fabrication of materials at atomic or nanoscale precision is to achieve some properties which may not exist in their bulk phases and which may qualify them for particular applications in new and relevant technologies. One way is to grow artificial crystal structures that are either intrinsically unstable in their bulk form or even do not exist in nature. An interesting example of such architectures is the arrangement of metallic superlattices to construct alternating monoatomic layers. The repeated stacking of different atomic layers of metallic elements is referred to as artificially-ordered layered films (ALF) [2, 4]. The ALF either exist in their corresponding bulk phase like FePd [5] or do not e.g., FeCu [4, 6], FeAu [7], AuCu [8], FeNi [2, 9–17], CoRu [18], AuNi [19]. In the latter case they are unstable or metastable at room temperature once engineered. These ALF fabricated with atomic-scale accuracy might have fascinating magnetic properties, which could be used in implicit technologies. For example, $L1_0$ FeNi fabricated by alternating deposition has high values of saturation magnetization, coercivity, perpendicular anisotropy energy and a quite high Curie temperature [2]. Another feature of these ALF is that a different layer stacking for the same material may provide different magnetic properties. For instance, in the case of FeNi ALF, it is reported that the Ni-sandwiched Fe layer has a higher magnetic anisotropy than the Fe-sandwiched Ni layer of the same thickness [15].
In this article, we are specifically interested in the ALF of Ni and Mn to have a model system of an antiferromagnet (AFM) which does not exist naturally. We prefer epitaxial growth to control properly the film's structural properties, mainly the interfaces. Using thermal evaporation, very little work has been reported on the growth of ALF and their multilayers [1, 3]. There are three basic pre-requisites to grow

ALF successfully along the film normal: (i) each layer thickness should be regulated on an atomic scale, (ii) interdiffusion should be sufficiently suppressed for independently deposited elements, and (iii) deposited materials should form a layered structure following a layer-by-layer growth. In this study, we fabricated ALF of Ni and Mn with atomic precision, i.e., in a layer-by-layer growth mode on a $Cu_3Au(001)$ single crystal. The two metallic elements Ni and Mn were selected in our work because they are well investigated as single-crystalline AFM systems in the form of disordered alloys (Ni_xMn_{100-x}) [20–26]. Tetragonally distorted NiMn disordered alloys grow in different directions on two different single crystalline substrates. On Cu(001) they grow along their a axis, while on $Cu_3Au(001)$ the growth is along the c axis, yielding a uniform structural domain [25, 27]. Ni_xMn_{100-x} shows layer-by-layer growth on $Cu_3Au(001)$ [25]. On top of each film 10 ML ferromagnetic (FM) Co is deposited, which grows epitaxially on top of the Ni_xMn_{100-x} or the Mn AFM layers [20, 25, 27] and exhibits an in-plane easy axis of magnetization. [Ni_n/Mn_m] multi-stacks with n = 1 ML and m between 1 and 3 ML were prepared with total thicknesses of 10, 12, 15, and 20 ML (Fig.1). In parallel, for its comparison, disordered Ni_xMn_{100-x} alloy films of the same thicknesses and almost the same Ni content were prepared, to better understand the structural and magnetic properties for both of these systems.

2 Results and Discussion

Figure 1 shows schematic illustrations of the three types of ALF ultrathin films that have been prepared on $Cu_3Au(001)$ at T = 300 K, keeping the thickness of Ni to 1 ML while changing the thickness of the Mn layers from 1 to 3 ML.

For each of these three geometries of ALF, four different thicknesses have been grown, namely 10, 12, 15 and 20 ML, by adjusting the thickness of the last Mn layer, which changes the overall concentration of the ALF film. For comparison, films of disordered Ni_xMn_{100-x} alloys with the same thicknesses and the same concentration were prepared. Our aim was that in films of the same thickness, the disordered alloy should have the same Ni content as the center of the ALF. For 20 ML of ALF, we have additionally investigated samples in which we exchanged the sequence of Ni and Mn deposition.

The growth of Ni and Mn in ALF and that of disordered AFM alloy Ni_xMn_{100-x} at T=300 K was monitored and controlled by means of medium-energy electron diffraction (MEED) intensity oscillations.

Ni always grows in layer-by-layer fashion on $Cu_3Au(001)$ up to 20 ML [27,28]. Mn has also been reported to grow in layer-by-layer growth mode [29]. However, this was not the case for all growth conditions [27, 30–33]. In our case, MEED oscillations for the growth of $Mn/Cu_3Au(001)$ up to thicknesses above 60 ML could be observed [34].

An oscillating MEED intensity, which is a fingerprint of a layer-by-layer growth mode, was found for all disordered Ni_xMn_{100-x} alloys and the ALF. Some of them are shown in Fig. 2. For the ALF, switching of the shutter between sources of Ni and Mn evaporation is marked by dashed vertical bars. Blue vertical bars correspond to 1 ML filling of Ni, while red vertical bars correspond to 1 ML (black curve), 2 ML (red curve) and 3 ML (blue curve) filling of Mn. A difference in the MEED oscillation amplitudes for Ni and Mn in the ALF were only observed for the initial growth of films with $m = 1$ (e.g., the black curve in Fig. 2), where Mn depicts higher amplitudes than Ni. This might be attributed to the smaller mismatch of Mn with the substrate $Cu_3Au(001)$ compared to Ni. A similar behavior has been reported for Fe/Cu ALF (lattice mismatch between *fcc* Fe and *fcc* Cu) on Cu(001), where Cu showed the higher amplitude of oscillations than Fe [1]. For alloy films, the amplitude of the oscillations decreases with film thickness, while it increases for ALF. The reason for this will be discussed later.

Figure 3 shows low-energy electron diffraction (LEED) images of the substrate, pure Mn, disordered Ni_xMn_{100-x} alloy, and ALF, of 9 ML thickness each. All the LEED images are taken at room temperature with a beam energy of 130 eV. The LEED patterns of ALF show a c(2×2) superstructure and sharper LEED spots compared to the disordered alloy films. The additional (2×2) superperiodicity of the ALF might come from a reconstruction induced by the Mn atoms, or from some Au segregation to the surface layer of these films, as already reported for thin Mn as well as for Co-Ni alloy films grown on top of $Cu_3Au(001)$ [28, 30, 35], or could be due to the buckling of either the surface layer or each layer [36].

Figure 4 (a) shows room-temperature LEED I(V) curves for 9 ML thick disordered Ni_xMn_{100-x} alloys and the corresponding ALF of 1 ML Ni/m ML Mn, deposited on $Cu_3Au(001)$. One can observe a shift of the peaks to higher energies for ALF compared to the corresponding disordered alloy films. The shift of the peaks to higher energies is also observed with increasing Ni content within both types of the prepared films. Figure 4 (b) shows the resulting interlayer spacing d versus overall Ni content x. With increasing Ni concentration, the interlayer distance decreases. It should be noted that in two of the ALF, namely 1 ML Ni/3 ML Mn and 1 ML Ni/1 ML Mn, we have a slightly lower overall Ni content (22.2% and 44.4%, respectively) than in the corresponding $Ni_{25}Mn_{75}$ and $Ni_{50}Mn_{50}$ disordered alloys because at 9 ML the growth stops with Mn instead of Ni. However, the local Ni concentration in the interior of the ALF is the same as in the disordered alloy films.

The interlayer distances are smaller for the ALF compared to the corresponding disordered alloys. The reason could be due to the densely packed structure of Ni and Mn sheets in which Mn (maybe Ni, too) exhibits some kind of buckling, either at the surface of the film, or possibly in each sheet inside the ALF [36]. The dashed lines at 1.88 Å and 1.76 Å indicate the interlayer distance for *fcc* $Cu_3Au(001)$, as experimentally obtained here, and for bulk $L1_0$ NiMn along the c-axis, respectively. For ALF of 1 ML Ni/1 ML Mn, d coincides with the value of the c-axis in bulk $L1_0$ NiMn.

Magnetic hysteresis loops are measured with longitudinal magneto-optical Kerr effect (MOKE) at different temperatures after field cooling with +25 mT from above the Néel temperature (T_N) of Mn and below the Curie temperature (T_C) of the Co, i.e., from ~500 K, which provided the exchange-bias shift along the negative field axis below the blocking temperature.

Figure 5 shows an example of temperature-dependent hysteresis loops. Here the samples are (a) 10 ML Co/15 ML Mn_2Ni_1 and (b) 10 ML Co/15 ML $Ni_{33}Mn_{67}/Cu_3Au(001)$. Nearly rectangular-shaped loops are obtained in both cases, in which a coercivity (H_c) enhancement with decreasing temperature can be observed. Already with the bare eye one can see that the exchange-bias shift, which becomes apparent at the lowest temperatures, is larger for the ALF shown in panel (a) than for the disordered alloy film in panel (b).

The evaluation of the temperature dependence of the coercivity H_c (positive field axis) and the exchange-bias field H_{eb} (negative field axis) of 15 ML thick films of pure Mn, $Ni_{25}Mn_{75}$, $Ni_{33}Mn_{67}$, $Ni_{50}Mn_{50}$ disordered alloys and 3 ML Mn/1 ML Ni, 2 ML Mn/1 ML Ni, 1 ML Mn/1 ML Ni ALF grown on $Cu_3Au(001)$ in contact with in-plane magnetized FM Co is presented in Fig. 6. Note that one additional 1 ML Mn / 1 ML Ni ALF of different thickness, namely 16 ML, is shown together with the other films to see the influence of 1 additional ML of Mn on top for this film. The exchange-bias fields of the ALF samples are consistently higher at all temperatures than those of the corresponding disordered Ni_xMn_{100-x} alloys. The same is true for their coercivities, except in the equiatomic case, where they are nearly equal. We define as the blocking temperature T_b for exchange bias the temperature below which the exchange-bias field deviates significantly from zero [20]. The blocking temperatures of the ALF and the disordered alloy samples are indicated by arrows with dotted and solid lines, respectively. The blocking temperatures of the ALF are distinctly higher than the ones of the corresponding disordered alloy films.

With decreasing Ni concentration, H_{eb} and T_b shift to higher values in both types of films, ALF and disordered alloys, for the latter consistent with Ref. [22]. Interestingly, adding one ML of Mn to the 1 ML Mn / 1 ML Ni film, making it in total 16 ML, results in higher values for coercivity, exchange-bias field, and T_b compared to 15 ML ALF and also to the 15 ML thick equiatomic disordered alloy.

Figure 7 shows the temperature-dependent behavior of the coercivity (positive field axis) and exchange-bias field (negative field axis) of 20 ML thick films of pure Mn, $Ni_{25}Mn_{75}$, $Ni_{33}Mn_{67}$, $Ni_{50}Mn_{50}$ disordered alloys and 3 ML Mn/1 ML Ni, 1 ML Ni/3 ML Mn, 2 ML Mn/1 ML Ni, 1 ML Ni/2 ML Mn, 1 ML Mn/1 ML Ni, 1 ML Ni/1 ML Mn ALF grown on $Cu_3Au(001)$ in contact with in-plane magnetized FM Co. H_{eb} as well as T_b increase with decreasing Ni concentration for both, disordered alloy and ALF. For each concentration, the bilayers containing ALF show much higher H_{eb} as well as T_b and the same is true for the coercivity values compared to the bilayers with disordered Ni_xMn_{1-x} films. Further data, all showing the same trend, are presented in the Supporting Information. It is worth noting that the exchange-bias field of the 2 ML Mn/1 ML Ni and 3 ML Mn/1 ML Ni ALF exceeds the one of all disordered alloys, in-

cluding that of pure Mn. The introduction of vertical order into the NiMn AFM layer is thus a means of further boosting its exchange-bias effect.

Within the ALF, when Mn is evaporated first and then Ni on top, even higher values of H_{eb} as well as T_b are observed. This means if the growth of the ALF stops with Mn layers on top rather than Ni layers, then it also boosts H_{eb} as well as T_b, as it is the case, too, in 16 ML ALF of 1 ML Mn/ 1 ML Ni, when compared to 15 ML of the same film (Fig. 6). The equiatomic $Ni_{50}Mn_{50}$ disordered film hardly shows any exchange bias, which is in agreement with the work of Khan *et al.* [27], but interestingly equiatomic ALF, i.e., 1 ML Mn/1 ML Ni and 1 ML Ni/1 ML Mn, show a sizeable exchange-bias field and T_b of 160 K and 220 K, respectively. Exchange bias for the equiatomic alloy films before was only found in 35 ML thick films [27]. The $Ni_{33}Mn_{67}$ disordered alloy film has a T_b of 260 K, while the ALF with nearly the same overall Ni content show T_b of 340 K (2 ML Mn/1 ML Ni) and 400 K (1 ML Ni/2 ML Mn), respectively. In the latter case we have one extra monolayer of Mn on top of the film compared to the former case, which means 5% more Mn overall in one geometry than in the other. Again, the additional top Mn layer is enlarging H_{eb} as well as T_b. $Ni_{25}Mn_{75}$ shows the second-highest value of the blocking temperature (340 K) among the disordered alloy films, after pure Mn (425 K). The ALF with nearly the same content of Ni and Mn as the $Ni_{25}Mn_{75}$ disordered alloy yields even higher values of coercivity, exchange-bias field, and a T_b of 400 K (3 ML Mn/1 ML Ni) and 425 K (1 ML Ni/3 ML Mn).

We relate the higher exchange-bias field and blocking temperature of the vertically ordered ALF compared to the disordered alloy films to the structural differences detected by LEED and LEED I(V). The smaller average interlayer distance in the ALF leads to a stronger exchange coupling within the AFM layer. Exchange bias originates from uncompensated pinned magnetic moments within the AFM, which couple to the FM layer. Since these pinned magnetic moments are distributed throughout the AFM layer [23, 37–41], their coupling to the FM layer and thus the exchange-bias field depends on the intra-AFM exchange interaction. A smaller average vertical atomic spacing enhances the exchange interaction in the AFM layer.

Besides the stronger exchange interaction due to the decreased perpendicular interplanar distance in the ALF samples, also other effects, for example related to the more ordered nature of the ALF films, could contribute to the enhancement of H_{eb}, T_b, and H_C. Although the detailed nature of the pinning centers is not known, intuitively one would assume that their number is greater in a chemically disordered alloy than in the ALF. However, in principle it could also be the opposite. For example, parts of the Ni layers in the ALF could act as uncompensated pinned moments, enhancing the exchange bias. This could be one possibility of how the interface between Ni and Mn affects the magnetic properties of the sample.

The reason for the vertical contraction of the ALF layers, which in view of the lateral lattice constant being fixed by the epitaxy to the substrate leads to an increase in atomic density, could be a vertical buckling of the films induced by the Mn-rich layers in the ALF. Mn has a smaller atomic density than the Cu_3Au substrate, as seen from the larger vertical lattice spacing of pure Mn films on $Cu_3Au(001)$ compared to the substrate (Fig. 4 (b)). A monoatomic layer of Mn atoms on $Cu_3Au(001)$ will thus tend to buckle vertically. If such a buckling repeats coherently through the other Mn layers of the ALF, this might lead to a higher atomic density than in disordered MnNi alloys.

LEED patterns of the clean $Cu_3Au(001)$ substrate are characterized by the (1/2, 1/2) spots of the $c(2 \times 2)$ superstructure relating to the $L1_2$ structure of Cu_3Au. The same pattern is also found with similar intensity and sharpness for the ALF. A possible explanation is that the substrate alloy structure seeds the buckling of the ALF. Note that a much weaker $c(2 \times 2)$ superstructure is also seen in the LEED patterns of some of the disordered alloy films. Its presence in disordered Ni_xMn_{100-x} alloy films and pure Mn films on $Cu_3Au(001)$ has been discussed before [25, 30, 31].

The layer-by-layer growth opens the way to atomic-scale manipulation of the interface roughness [42]. In the present study, we have stopped the growth of the Ni and Mn layers at the maxima of the specularly reflected (00)-spot MEED intensity, minimizing such the roughness. It could be interesting to see how the magnetic properties evolve if the interface roughness is increased.

Altogether the blocking temperature extends to higher values with decreasing Ni concentration in all samples (shown with the colored arrows), which confirms previous results on this system [27].

The bilayers with ALF where Mn is evaporated on top have higher H_{eb} and higher T_b compared to those where the top layer is Ni. Furthermore, in [Ni/Mn] ALF in which Mn is evaporated first, the blocking temperature, exchange-bias field and coercivity are higher for the same thicknesses compared to the ALF where Ni is evaporated first. There could be many reasons for that, among them that a few ALF for which we start with evaporating Mn and end up with Mn have slightly more Mn overall compared to the [Mn/Ni] case when Ni is evaporated first (see Fig. 1) and more Mn means a larger number of itinerant *d*-like electrons for the same thickness and hence enhanced H_{eb}, T_b, and H_c. For a reference we can also take a look at pure Mn in the same graph (Fig. 7) as well as in Fig. 6 and Fig. S1 of the Supporting Information, which show higher values of H_{eb} than any other Ni_xMn_{100-x} alloy film for 20 ML thickness. Similarly, the observation when adding one ML of Mn to the AFM layer can be explained. It has a two-fold effect: On the one hand, it increases the effective thickness of the AFM layer, which, due to finite-size scaling, directly affects T_N, as has been shown before for disordered NiMn alloys [22]. On the other hand, it raises the overall Mn concentration in the film, which also enhances T_N. A higher T_N results in a higher stability of the AFM spin structure, a stronger coupling to the FM layer at a given temperature, and thus to larger H_{eb}, T_b, and H_C [22].

3 Conclusion

We have investigated the growth and structural properties of single-crystalline ultrathin [Ni/Mn] ALF in comparison with the corresponding disordered Ni_xMn_{100-x} alloy films on $Cu_3Au(001)$. For all samples our results revealed good epitaxial layer-by-layer growth at a substrate temperature of 300 K.
The average perpendicular interlayer spacing of the ALF is up to about 1% smaller than the one of the corresponding disordered alloys. This could result from a coherent regular buckling of the atomic layers in the ALF, induced by the Mn layers, which would be consistent with the stronger $c(2 \times 2)$ superstructure spots observed in the LEED patterns from the [Ni/Mn] ALF. This parallels a generally stronger exchange bias, higher coercivity, and higher blocking temperature in the ALF compared to the disordered alloy films of the same thickness and overall composition. We attribute this to a stronger exchange coupling across the layers in the antiferromagnet for the smaller interlayer spacing.

4 Experimental Section

Sample preparation and characterization were performed under ultrahigh vacuum conditions with a base pressure of 2 $\times 10^{-10}$ mbar and 8 $\times 10^{-10}$ mbar during the deposition of the films. The chemical cleanliness of the single-crystalline $Cu_3Au(001)$ substrate (with miscut $\leq 0.1°$) was verified by Auger electron spectroscopy (AES) after repetitive cycles of sputtering with Argon (1.2 keV) at 300 K and annealing at 820 K for 5 min and then at 800 K for 30 min to get a smooth and well-ordered surface. Using an Oxford Instruments four-pocket evaporator, Co and Ni were deposited from high-purity rods (99.99%), while Mn was evaporated from a Ta crucible filled with pure Mn flakes (99.98%) by electron-beam-assisted thermal evaporation at 300 K. The electron beam was focused on the tip of the 2 mm rod and on top of the 6 mm crucible, for the Co/Ni and Mn evaporation, respectively, which are set to positive high voltage and held in a water-cooled system. The Ni_xMn_{100-x} films were prepared by the simultaneous evaporation of Ni and Mn on $Cu_3Au(001)$ while for the preparation of ALF of Ni and Mn, a shutter in front of the evaporator was used to precisely control the evaporation of the materials and to open only either the Ni or the Mn evaporator at a time. In the alloy samples, the Ni concentration x was varied by optimizing the individual deposition rates, while in the ALF case the evaporation rate is kept constant all the time within the uncertainity of ~3% related to flux variations. The growth of the films was checked by counting the oscillations in the (0, 0)-spot intensity of MEED recorded during evaporation. The film structure was probed by LEED. The film's lattice spacing along the surface normal was obtained from the kinematic analysis of LEED intensity-versus-energy [LEED I(V)] curves of the (0, 0) LEED spot at $\theta = 5°$ electron incidence from the surface normal. AES was used to confirm the cleanliness of the substrate and the Ni concentration in the Ni_xMn_{100-x} alloys and in the ALF. The magnetic properties

were measured by *in-situ* MOKE. Linearly polarized laser light from a laser diode of 1 mW power and 632 nm wavelength was used. A field-cooling procedure was applied to the samples to set possible exchange bias. Temperature–dependent hysteresis loops were measured using longitudinal MOKE after field-cooling with + 25 mT from above T_N of Mn and below T_C of the Co film, i.e., from 500 K, which provided an exchange-bias shift along the negative field direction. The minimum temperature attained for the MOKE measurements using liquid-helium cooling was 50 K.

Supporting Information
Supporting Information is available from the Wiley Online Library or from the author.

Acknowledgements
T. Shinwari is grateful for financial support during his stay in Berlin by the Senator of District Khyber (Ex-FATA), Pakistan, and Freie Universität Berlin. We thank Uwe Lipowski for technical assistance. M. Y. Khan thanks the Alumni Office of Freie Universität Berlin for financial support during his stay in Berlin through the Research Alumni Program.

References

[1] J. Shen, Z. Gai, J. Kirschner, *Surface Science Reports* **2004**, *52*, 5-6 163.

[2] S. Mandal, M. Debata, P. Sengupta, S. Basu, *Critical Reviews in Solid State and Materials Sciences* **2022**, 1–23.

[3] A. Sáenz-Trevizo, A. M. Hodge, *Nanotechnology* **2020**, *31*, 29 292002.

[4] S. S. Manoharan, M. Klaua, J. Shen, J. Barthel, H. Jenniches, J. Kirschner, *Physical Review B* **1998**, *58*, 13 8549.

[5] V. Gehanno, Y. Samson, A. Marty, B. Gilles, A. Chamberod, *Journal of Magnetism and Magnetic Materials* **1997**, *172*, 1-2 26.

[6] W. Kuch, M. Salvietti, X. Gao, M. T. Lin, M. Klaua, J. Barthel, C. V. Mohan, J. Kirschner, *Physical Review B* **1998**, *58*, 13 8556.

[7] K. Takanashi, S. Mitani, M. Sano, H. Fujimori, H. Nakajima, A. Osawa, *Applied Physics Letters* **1995**, *67*, 7 1016.

[8] M. Dynna, A. Marty, B. Gilles, G. Patrat, *Acta Materialia* **1997**, *45*, 1 257.

[9] R. Dawn, M. Zzaman, R. R. Bharadwaj, C. Kiran, R. Shahid, V. K. Verma, S. K. Sahoo, K. Amemiya, V. R. Singh, *Journal of Sol-Gel Science and Technology* **2021**, *99*, 3 461.

[10] K. Kawaguchi, T. Miyamachi, T. Iimori, Y. Takahashi, T. Hattori, T. Yokoyama, M. Kotsugi, F. Komori, *Physical Review Materials* **2020**, *4*, 5 054403.

[11] V. Thiruvengadam, B. B. Singh, T. Kojima, K. Takanashi, M. Mizuguchi, S. Bedanta, *Applied Physics Letters* **2019**, *115*, 20 202402.

[12] M. Saito, H. Ito, Y. Suzuki, M. Mizuguchi, T. Koganezawa, T. Miyamachi, F. Komori, K. Takanashi, M. Kotsugi, *Applied Physics Letters* **2019**, *114*, 7 072404.

[13] K. Takanashi, M. Mizuguchi, T. Kojima, T. Tashiro, *Journal of Physics D: Applied Physics* **2017**, *50*, 48 483002.

[14] T. Kojima, M. Mizuguchi, K. Takanashi, *Thin Solid Films* **2016**, *603* 348.

[15] M. Sakamaki, K. Amemiya, *Applied Physics Express* **2011**, *4*, 7 073002.

[16] M. Mizuguchi, S. Sekiya, K. Takanashi, *Journal of Applied Physics* **2010**, *107*, 9 09A716.

[17] T. Shima, M. Okamura, S. Mitani, K. Takanashi, *Journal of Magnetism and Magnetic Materials* **2007**, *310*, 2 2213.

[18] K. Takanashi, K. Himi, S. Mitani, M. Yamaguchi, D. H. Ping, K. Hono, H. Fujimori, *Surface Science* **2001**, *493*, 1-3 713.

[19] G. Abadias, I. Schuster, A. Marty, B. Gilles, T. Deutsch, *Journal of crystal growth* **2001**, *222*, 3 685.

[20] T. Shinwari, I. Gelen, Y. A. Shokr, I. Kumberg, I. Ikramullah, M. Sajjad, W. Kuch, M. Y. Khan, *Physica Status Solidi (RRL)–Rapid Research Letters* **2021**, *15* 2100195.

[21] I. Kumberg, E. Golias, N. Pontius, R. Hosseinifar, K. Frischmuth, I. Gelen, T. Shinwari, S. Thakur, C. Schüssler-Langeheine, P. M. Oppeneer, W. Kuch, *Physical Review B* **2020**, *102*, 21 214418.

[22] M. Y. Khan, C. B. Wu, S. K. Kreft, W. Kuch, *Journal of Physics: Condensed Matter* **2013**, *25*, 38 386005.

[23] M. Y. Khan, C. B. Wu, W. Kuch, *Physical Review B* **2014**, *89*, 9 094427.

[24] M. Y. Khan, C. B. Wu, M. Erkovan, W. Kuch, *Journal of Applied Physics* **2013**, *113*, 2 023913.

[25] W. A. A. Macedo, P. L. Gastelois, M. D. Martins, W. Kuch, J. Miguel, M. Y. Khan, *Physical Review B* **2010**, *82*, 13 134423.

[26] M. Reinhardt, J. Seifert, M. Busch, H. Winter, *Physical Review B* **2010**, *81*, 13 134433.

[27] M. Y. Khan, Ph.D. thesis, Freie Univärsität Berlin, **2012**.

[28] B. Y. Wang, W. C. Lin, Y. W. Liao, K. J. Song, M. T. Lin, *Surface Science* **2006**, *600*, 19 4517.

[29] B. Schirmer, B. Feldmann, A. Sokoll, Y. Gauthier, M. Wuttig, *Physical Review B* **1999**, *60*, 8 5895.

[30] W. C. Lin, T. Y. Chen, L. C. Lin, B. Y. Wang, Y. W. Liao, K. J. Song, M. T. Lin, *Physical Review B* **2007**, *75*, 5 054419.

[31] W. C. Lin, L. C. Lin, T. Y. Chen, B. Y. Wang, K. J. Song, M. T. Lin, *Journal of Applied Physics* **2005**, *97*, 10 10K112.

[32] A. Tange, C. Gao, C. T. Chiang, M. T. Lin, W. Wulfhekel, J. Kirschner, *Materials Transactions* **2015**, *56*, 9 1484.

[33] C. Tieg, W. Kuch, S. G. Wang, J. Kirschner, *Physical Review B* **2006**, *74*, 9 094420.

[34] T. Shinwari, Ph.D. thesis, Freie Universität Berlin, **2022**.

[35] W. C. Lin, B. Y. Wang, Y. W. Liao, K. J. Song, M. T. Lin, *Physical Review B* **2005**, *71*, 18 184413.

[36] C. L. Gao, A. Ernst, A. Winkelmann, J. Henk, W. Wulfhekel, P. Bruno, J. Kirschner, *Physical Review Letters* **2008**, *100*, 23 237203.

[37] P. Miltényi, M. Gierlings, J. Keller, B. Beschoten, G. Güntherodt, U. Nowak, K. D. Usadel, *Physical Review Letters* **2000**, *84*, 18 4224.

[38] U. Nowak, K. D. Usadel, J. Keller, P. Miltényi, B. Beschoten, G. Güntherodt, *Physical Review B* **2002**, *66*, 1 014430.

[39] J. Keller, P. Miltényi, B. Beschoten, G. Güntherodt, U. Nowak, K. D. Usadel, *Physical Review B* **2002**, *66*, 1 014431.

[40] I. K. Schuller, R. Morales, X. Batlle, U. Nowak, G. Güntherodt, *Journal of Magnetism and Magnetic Materials* **2016**, *416* 2.

[41] M. Y. Khan, Y. A. Shokr, W. Kuch, *Journal of Physics: Condensed Matter* **2019**, *32*, 7 075801.

[42] W. Kuch, L. I. Chelaru, F. Offi, J. Wang, M. Kotsugi, J. Kirschner, *Nature Materials* **2006**, *5*, 2 128.

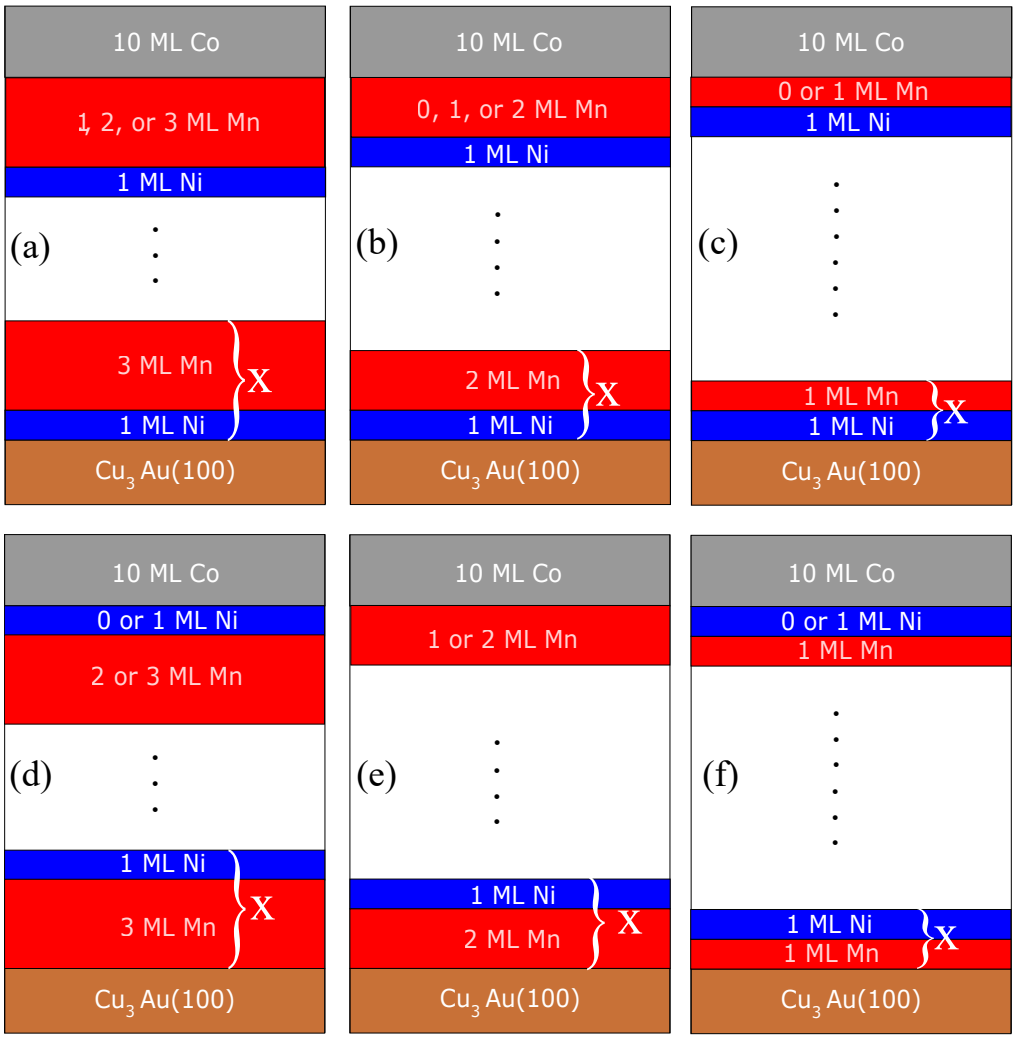

Figure 1: Schematic illustration of ALF of **m** ML Mn/1 ML Ni/Cu_3Au(001) (a–c) and 1 ML Ni/**m** ML Mn/Cu_3Au(001) (d–f); where **m** = 3 (a) and (d), **m** = 2 (b) and (e), **m** = 1 (c) and (f). The total thickness of these stacks is kept as 10, 12, 15 and 20 ML. 10 ML FM Co is always evaporated on top of these films for magnetic characterization.

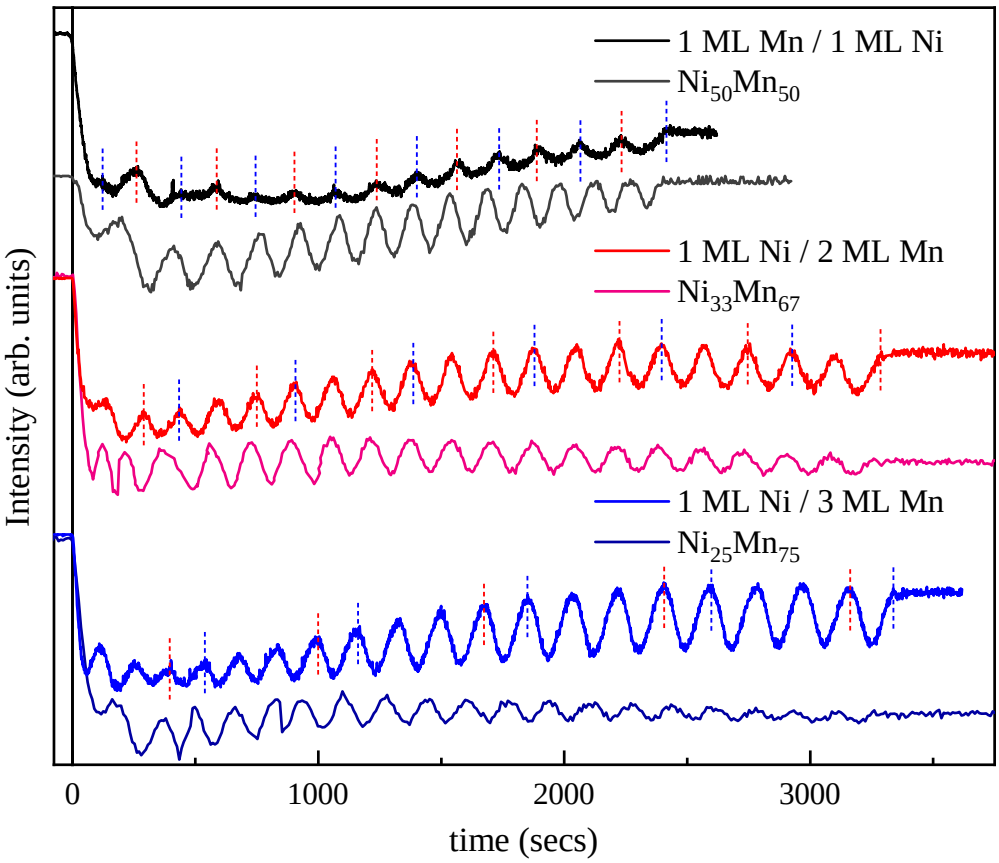

Figure 2: MEED oscillations for 15 and 20 ML ALF and corresponding disordered Ni_xMn_{100-x} alloy films on $Cu_3Au(001)$. For the ALF, the switching of the shutter between sources of Ni and Mn evaporation is marked with dashed vertical bars. The blue bar corresponds to 1 ML filling of Ni, while the red bar correlates to 1 ML (black curve), 2 ML (red curve), and 3 ML (blue curve) filling of Mn. For the disordered alloy films, the amplitude of the oscillations during the deposition decreases with increasing Mn content, while in the case of ALF, it depends on the Ni and Mn sequence. Depositing Ni first in the ALF (black curve) leads to a smaller amplitude of the oscillations compared to films starting with the deposition of Mn (red and blue curves).

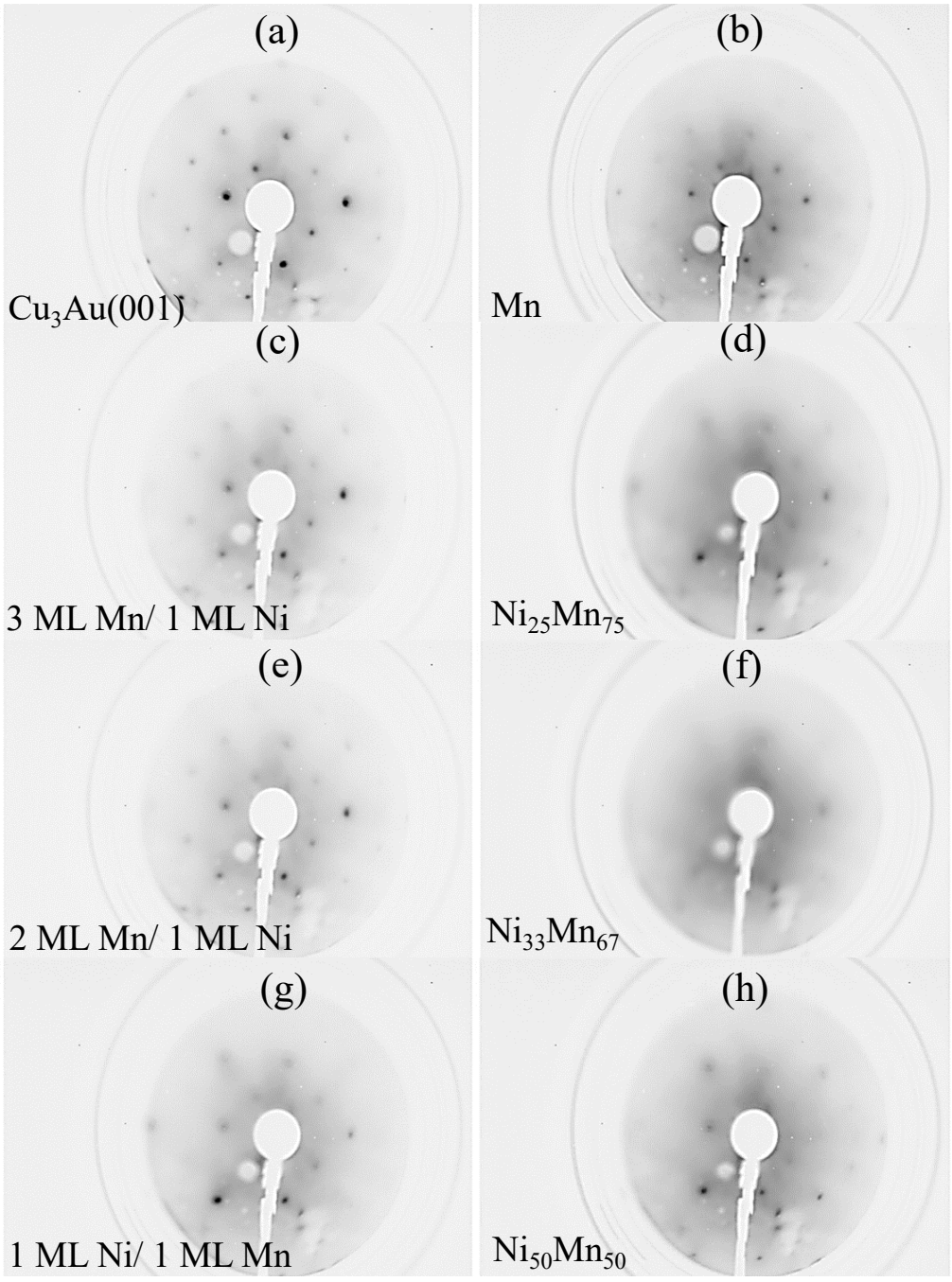

Figure 3: LEED patterns of (a) clean $Cu_3Au(001)$ and of 9 ML of (b) Mn, (c) 3 ML Mn/1 ML Ni, (d) $Ni_{25}Mn_{75}$, (e) 2 ML Mn/ 1 ML Ni, (f) $Ni_{33}Mn_{67}$, (g) 1 ML Mn/1 ML Ni, and (h) $Ni_{50}Mn_{50}$. All LEED images are taken at room temperature with a beam energy of 130 eV.

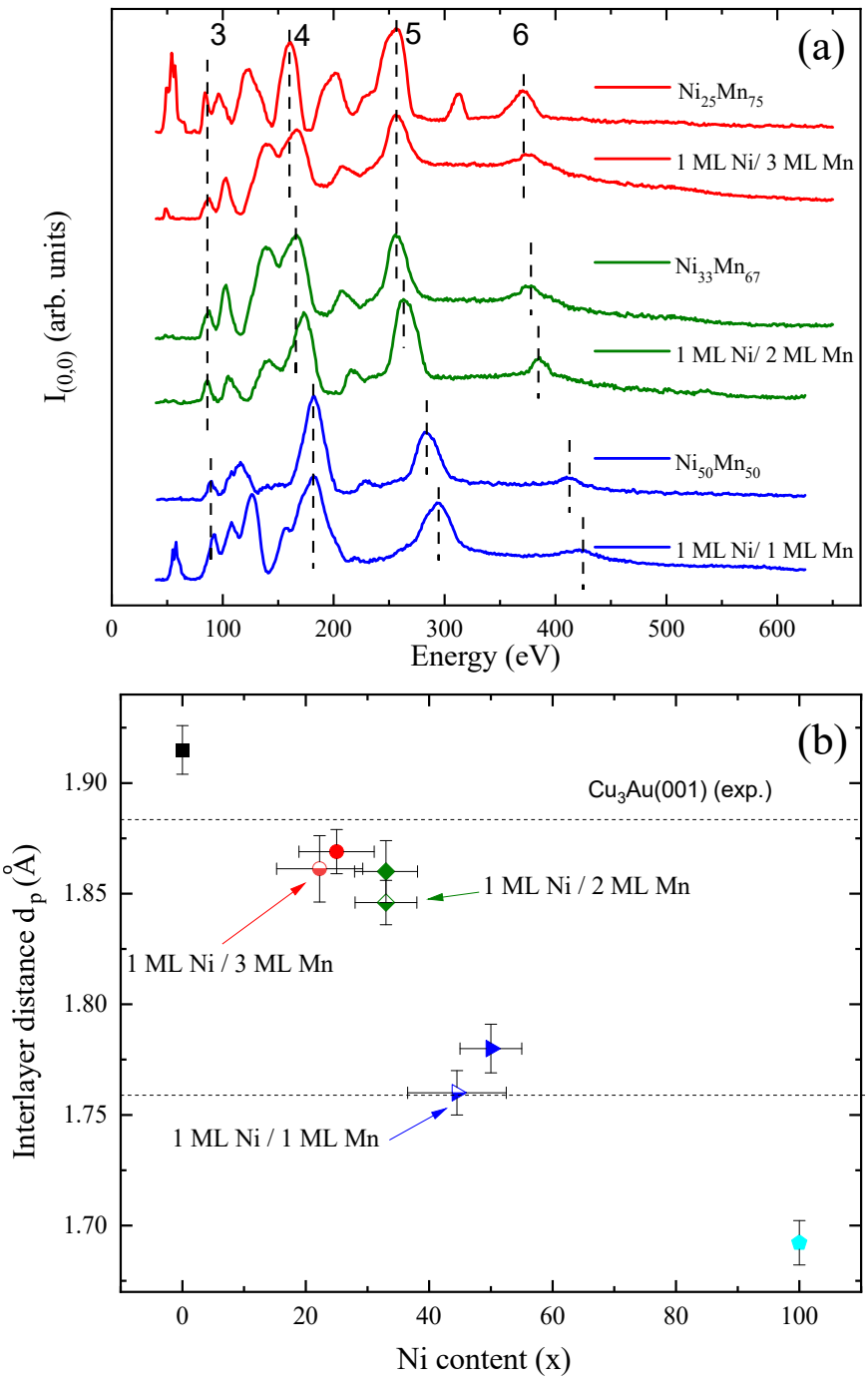

Figure 4: (a) Room-temperature LEED I(V) curves for 9 ML thick disordered Ni_xMn_{100-x} and ALF of 1 ML Ni/**m** ML Mn/Cu_3Au(001), where **m** ranges from 1 to 3. The numbers are the indices denoting the integer numbers of the single-scattering Bragg peaks indicated by the dashed lines. Note the shift of the peaks to higher energies for ALF compared to the corresponding disordered alloy films. A shift of the peaks to higher energies is also observed with increasing Ni content within both types of films. (b) Perpendicular interlayer distance d_p versus overall Ni content x. The dashed lines at 1.88 Å and 1.76 Å indicate the interlayer distances in *fcc* Cu_3Au(001), as experimentally obtained here, and in bulk $L1_0$ NiMn along the c axis, respectively. For ALF films of 1 ML Ni/1 ML Mn, d coincides with the value of the c axis in bulk $L1_0$ NiMn. For pure Mn ($x = 0$) and pure Ni ($x = 100$), the interlayer distances from LEED I(V) are 1.92 ± 0.01 Å and 1.69 ± 0.01 Å, respectively.

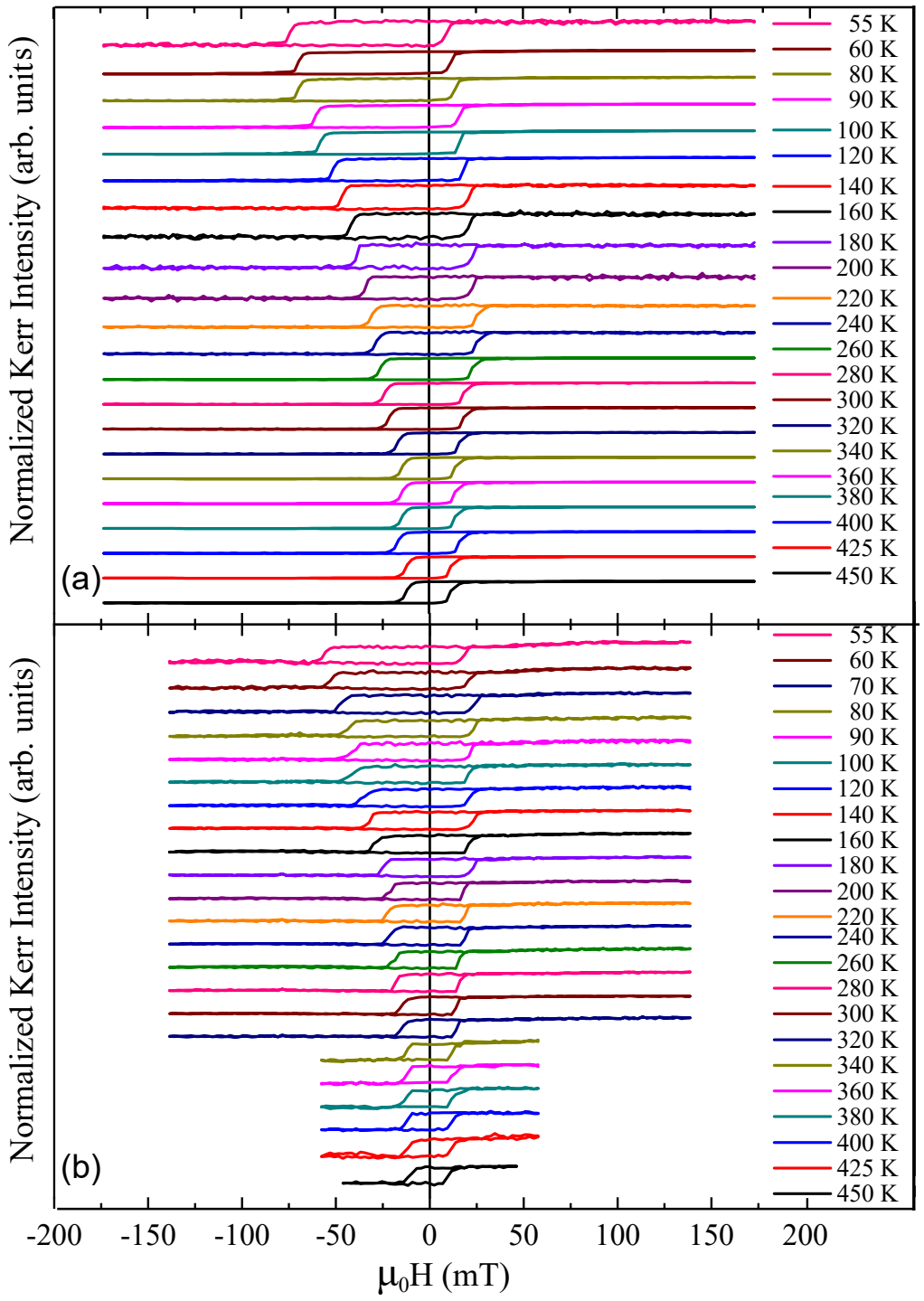

Figure 5: Normalized hysteresis loops for 10 ML Co on 15 ML thick (a) 2 ML Mn/1 ML Ni ALF and (b) $Ni_{33}Mn_{67}$ disordered alloy films, measured with longitudinal MOKE at different temperatures as indicated in the legend. The sample was field-cooled in +25 mT from ~500 K, above T_N of Mn and below the Curie temperature of the Co film.

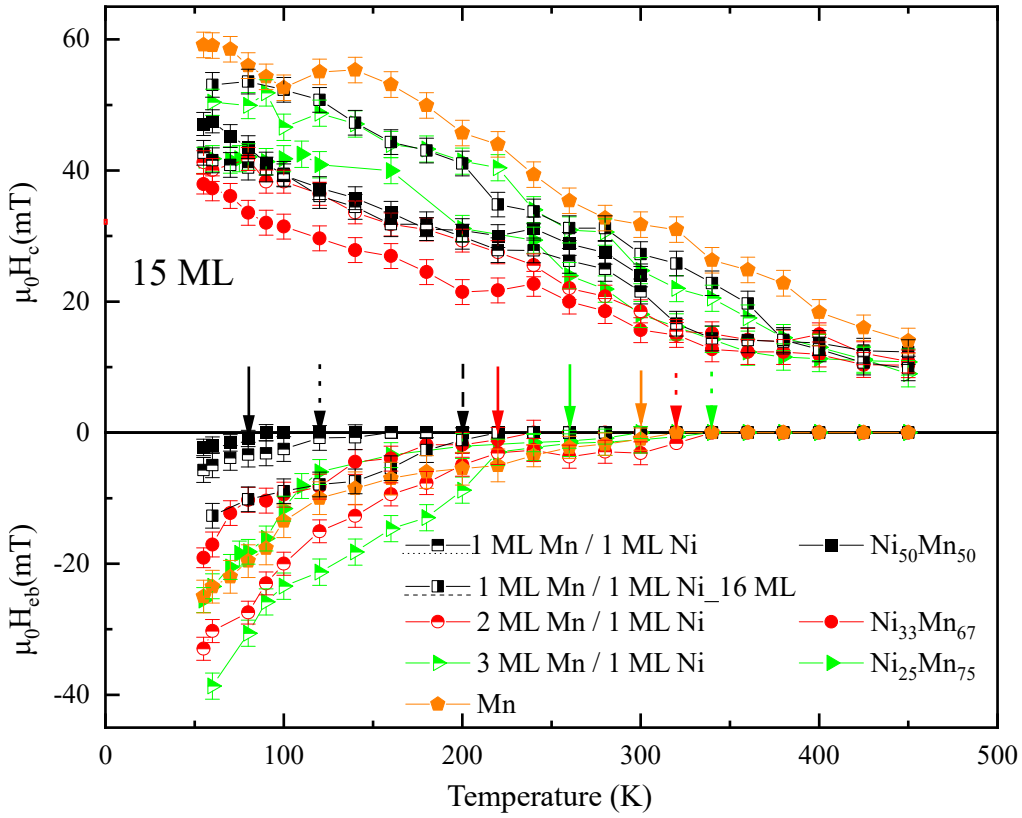

Figure 6: Temperature dependence of the coercivity (positive field axis) and exchange-bias field (negative field axis) of the bilayers with 15 ML thick films of pure Mn, $Ni_{25}Mn_{75}$, $Ni_{33}Mn_{67}$, $Ni_{50}Mn_{50}$ disordered alloys and those with 3 ML Mn/1 ML Ni, 2 ML Mn/1 ML Ni, 1 ML Mn/1 ML Ni ALF. Note that an additional 1 ML Mn/1 ML Ni ALF of 16 ML thickness is also prepared for comparison. The arrows indicate the blocking temperatures for the exchange-bias curves. Arrows with solid lines represent data for disordered alloy samples, arrows with dotted lines represent data for the ALF. The arrow with the dashed line corresponds to the 16-ML sample.

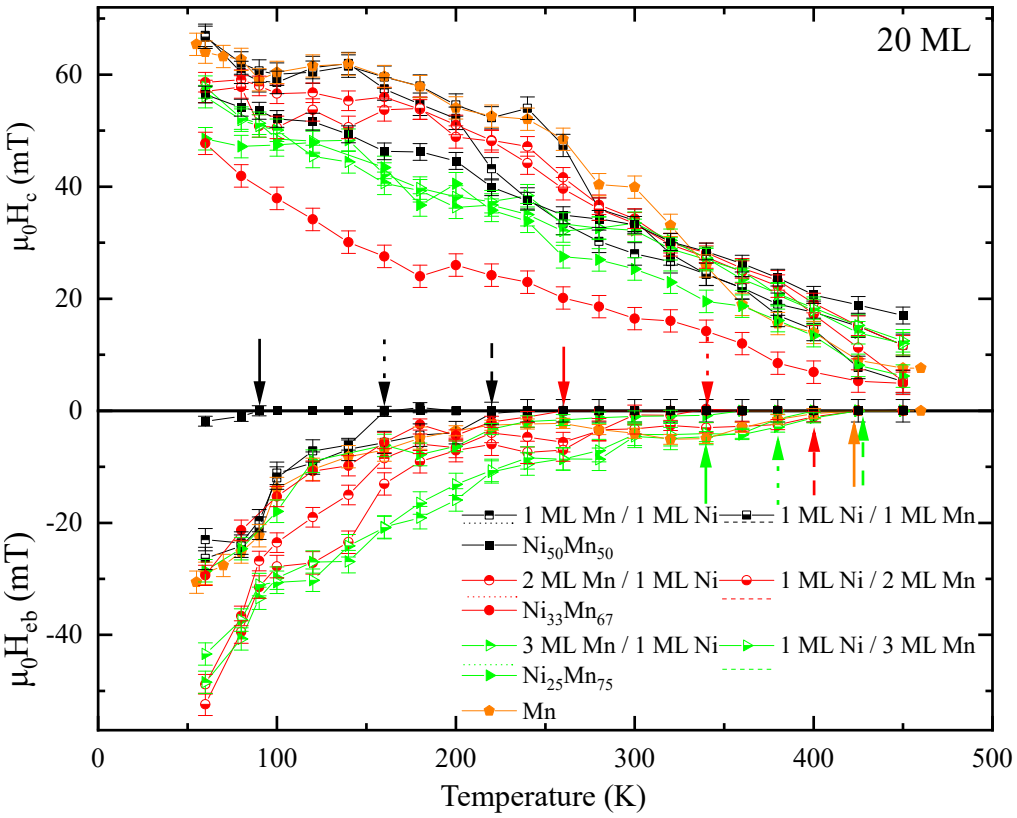

Figure 7: Temperature dependence of the coercivity (positive field axis) and exchange-bias field (negative field axis) of AFM/FM bilayers with AFM being 20 ML of pure Mn, $Ni_{25}Mn_{75}$, $Ni_{33}Mn_{67}$, $Ni_{50}Mn_{50}$ disordered alloys and 3 ML Mn/1 ML Ni, 1 ML Ni/3 ML Mn, 2 ML Mn/1 ML Ni, 1 ML Ni/2 ML Mn, 1 ML Mn/1 ML Ni, 1 ML Ni/1 ML Mn ALF. The arrows indicate the blocking temperatures for the exchange-bias curves. Arrows with solid lines represent data for disordered alloy samples, arrows with dotted lines represent data for the ALF in which Ni was evaporated first, while arrows with dashed lines represent data for the ALF in which Ni with Mn was evaporated first.